



Fermi National Accelerator Laboratory

FERMILAB-Conf-97/353

**Magnetic Field Analysis of the First Short Models of a High
Gradient Quadrupole for the LHC Interaction Regions**

G. Sabbi, J. Strait and A. Zlobin

*Fermi National Accelerator Laboratory
P.O. Box 500, Batavia, Illinois 60510*

S. Caspi

*Lawrence Berkeley National Laboratory
Berkeley, California*

October 1997

Proceedings of the *15th International Conference on Magnet Technology*,
Beijing, China, October 20-24, 1997

Magnetic Field Analysis of the First Short Models of a High Gradient Quadrupole for the LHC Interaction Regions

G. Sabbi, J. B. Strait, A. V. Zlobin
Fermilab, Batavia, Illinois, USA

S. Caspi
Lawrence Berkeley National Laboratory, Berkeley, California, USA

Abstract—In the frame of the U.S.-CERN collaboration for LHC, half of the high-gradient quadrupole magnets for the final focusing triplets of the interaction regions of LHC will be built at Fermilab. The design of these magnets has now reached an advanced stage, and the first two models are being fabricated. The paper describes the expected magnetic performance of these models, including short sample limits and field quality analysis for both the straight section and the end regions.

I. INTRODUCTION

Fermilab, Lawrence Berkeley National Laboratory and Brookhaven National Laboratory have formed a consortium to provide components for the Large Hadron Collider (LHC) to be built at CERN [1]. The U.S. contribution includes half of the high gradient quadrupoles (HGQ) for the inner focusing triplets. A new specification calls for a nominal field gradient of 200 T/m over a 70 mm aperture [2]. A high field quality is also required. Each magnet operates under a beam induced heat load of up to 40 Watts. To meet these severe constraints, a design based on a 2-layer, $\cos(2\theta)$ coil operating in superfluid helium at 1.9 K has been proposed [3]. A magnet model program aimed at validating and optimizing this design is under way. The fabrication of the first model (HGQS01) has progressed to an advanced stage, and the construction of a second model (HGQS02) with a modified end geometry is starting. The magnetic performance of the first two HGQ short models has been investigated in [4]-[8]. In this paper, a summary review of these results is presented.

II. DESIGN DESCRIPTION

The HGQ design is based on four two-layer coils connected in series. Each octant has two spacers, one for each layer, which allow a fine optimization of the field quality. The coils are surrounded by collar and yoke laminations. The coil prestress is entirely provided by the stainless steel collars, which have a width of 25 mm at the midplane. Eight rectangular gaps between collars and yoke house tuning shims for field quality adjustment. The iron yoke contributes about 10% of the central field. Its inner radius at the midplane is 92.56 mm; the outer radius is 200 mm. The resulting HGQ cross section is shown in Figure 1.

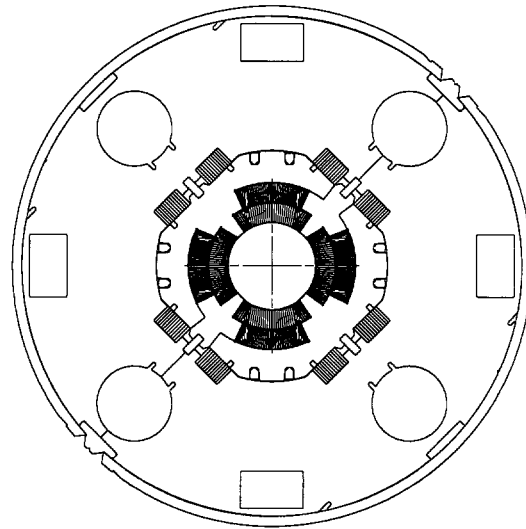


Fig. 1. HGQ cross-section.

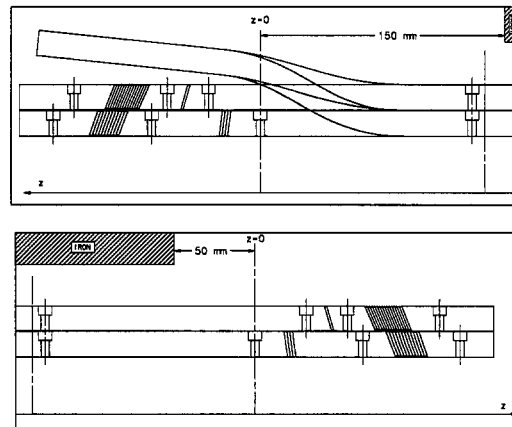


Fig. 2. Lead and return end geometry (HGQS01).

The design of the HGQ coil ends started with a magnetic optimization of the position of the conductor groups, followed by a mechanical optimization of the geometry of the end parts used to shape and constrain the conductors [9] [10]. The goal of the magnetic optimization is to provide low integrated harmonics, low peak magnetic field and minimum physical length. The field quality is optimized by adjusting the relative position of the conductor groups along the z axis, while the peak field is controlled by removing the iron yoke laminations from the last section of the magnet body. The mechanical optimization

aims at minimizing the strain energy of individual conductors within each group. Figure 2 shows the resulting cross-section at the pole angle for the magnet lead and return ends. The electrical connection between the two cables in the inner and outer layer of each coil is provided by an external splice in the lead end. This design has been adopted for the first HGQ short model (HGQS01). For the HGQS02 model, however, a modified end geometry was chosen, where the second-wound conductor group in the outer coil is shifted by 2 cm in the positive z direction. The modified geometry requires only minor changes of the end parts. It allows to reduce the peak field in the outer layer without compromising the field quality.

III. COMPUTER MODELS

The HGQ magnetic field analysis and optimization is performed using a combination of analytical and mesh programs: ROXIE [11], PKLBL [12], POISSON [13], FIGENDES [14]. Figure 3 shows a 3D ROXIE model of the HGQS01 lead end. In order to generate this model, a BEND-ROXIE interface has been written: it allows to transfer automatically the mechanically optimized geometry of the conductor groups to the magnetic analysis program.

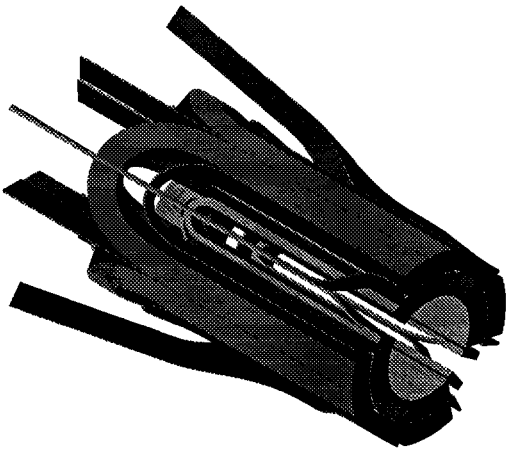


Fig. 3. ROXIE model of HGQS01 lead end. Only the part of the coil extending beyond the edge of the iron yoke is shown.

IV. SHORT SAMPLE LIMITS

The cable for the model magnet program uses SSC-type NbTi strand, with a critical current density of 2.75 kA/mm^2 at 5 T and 4.2 K. Table I reports the corresponding coefficients for the critical current of the inner and outer cables as function of field at 1.9 K. These coefficients have been calculated based on the conductor and cable parameters, and subsequently validated by comparison with experimental results carried out on samples of the inner and outer HGQ cables [15] [16].

Figure 4 shows the peak field load lines for the inner coil. For the straight section, a series of calculations at 2 kA intervals has been performed to take into account the

TABLE I
HGQ cable parameters at 1.9 K.

Inner cable		Outer cable	
$I_c(10 \text{ T})$	dI_c/dB	$I_c(8 \text{ T})$	dI_c/dB
14.1 kA	-4.5 kA/T	14.8 kA	-2.9 kA/T

iron saturation effects. The result for the end regions does not include magnetization effects: however, the distance from the edge of the iron yoke to the coil end is sufficiently large to ensure that the contribution of the iron yoke to the peak field can be neglected. Since the peak field occurs at the location of the first-wound conductor group, no significant difference between the two versions of the end design is observed. The resulting maximum current for the inner layer is 14.5 kA in the magnet body and 15 kA in the end regions.

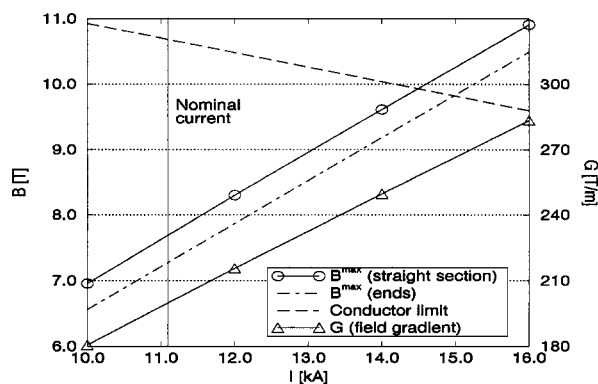


Fig. 4. Field load lines for the inner coil.

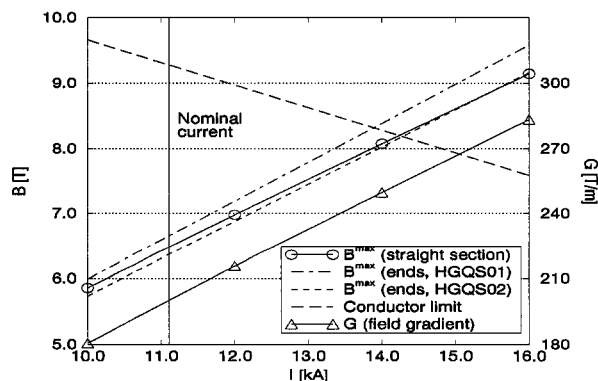


Fig. 5. Field load lines for the outer coil.

Figure 5 shows the field load lines for the outer coil. As can be seen, in the case of model HGQS01 the limit current in the outer layer is determined by the peak field in the ends. The high-field point is located at the innermost conductor of the second-wound group. The corresponding maximum current is 13.9 kA, as compared to a maximum current in the straight section of 14.2 kA. For the HGQS02 model, the modified end geometry allows to eliminate this effect, as shown in Figure 6. In this case, a maximum current of 14.3 kA can be achieved.

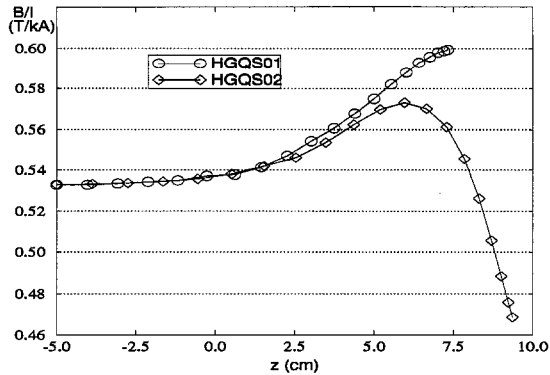


Fig. 6. Field load line as function of z for conductor with peak field (return end, outer layer) [8].

V. FIELD QUALITY ANALYSIS

A. Magnet body

In the straight section of the magnet, the field can be represented in terms of multipole coefficients defined according to the following expression:

$$B_y(x, y) + iB_x(x, y) = \sum_{n=1}^{\infty} (B_n + iA_n) \left(\frac{x + iy}{r_0} \right)^{n-1} \quad (1)$$

As customary for LHC magnets, the harmonics will be expressed in “units” of 10^{-4} of the main field component at a reference radius of 1 cm.

TABLE II
Expected field errors at collision (allowed harmonics).

Component	Mean	RMS spread
b_6	-0.09 [-0.14, +0.04]	0.06
b_{10}	+0.0003 [-0.0011, +0.0009]	0.0005
b_{14}	-0.00002 [\pm 0.00003]	0.00003

Table II shows the estimated systematic and random field errors at collision for the first three allowed harmonics in the HGQ magnet body. The systematic errors are expressed in terms of an expected value and an uncertainty range. The uncertainty is related to the accuracy of the modelling assumptions, and to magnetic measurement errors. The following sources of field errors have been analyzed:

Mechanical effects. Due to insufficient keystoneing of the cables, the coil curing mandrels do not provide a perfect radial constraint for some of the turns. It is expected that after curing the turns will be aligned to the outer mold radius. The uncertainty range corresponds to alignment of all turns to the inner mandrel radius.

The collared coil deformation during cooling down and springback under nominal prestress, as well as its deformation under Lorentz forces with respect to the warm unstressed geometry produce additional field errors. The Lorentz force effect is negligible at injection and maximal at collision.

Deviations from nominal prestress and turn/coil block displacements due to manufacturing tolerances contribute to the random errors, which have been estimated based on both a Monte Carlo simulation and the production data from LBQ and HERA [17] [18].

Magnetization effects. The coil magnetization is determined by the critical current density in the superconductor, filament diameter, Cu/Sc ratio, etc. This effect is maximal at injection and becomes negligible at collision. The uncertainty is related to the accuracy of the model and the parameters of the conductor under development.

The magnetization of the stainless steel collars and beam absorber produces current independent harmonics which depend on geometry and magnetic permeability. The measured collar permeability at 4.2 K is 1.003.

The yoke cross section was optimized to minimize the change in the harmonics due to iron saturation and to compensate the harmonics due to collar magnetization.

Magnetic measurements. The field quality of each HGQ magnet will be determined during magnetic measurements. Measurement errors contribute to the uncertainty in the systematic harmonics and to their RMS spread.

TABLE III
Correction of systematic harmonics by coil shimming.

Pole/Midplane Shim [μm]	Inner layer		Outer layer	
	Δb_6	Δb_{10}	Δb_6	Δb_{10}
-75/+75	-0.158	-0.00027	-0.024	-0.00003
+75/-75	+0.158	+0.00026	+0.024	+0.00002

The HGQ ground insulation scheme provides sufficient flexibility to allow correction of the systematic b_6 harmonic within the estimated range of uncertainty. The inner and outer coils can be independently shifted towards the pole or the midplane by up to 75 μm , with no prestress change. The corresponding variations of the systematic harmonics b_6 and b_{10} are listed in table III.

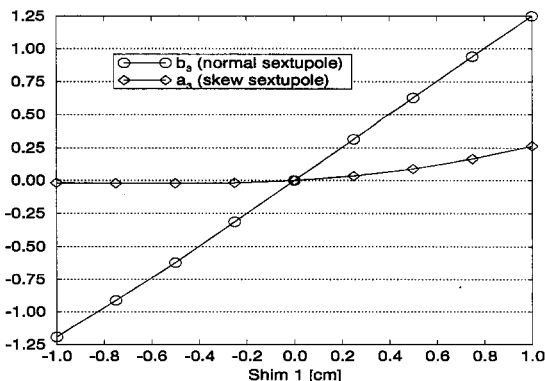


Fig. 7. Variation of normal and skew sextupole as function of the position of shim 1 (first quadrant) at $I=14\text{kA}$.

The HGQ design also incorporates tuning shims for correction of the low-order non-allowed harmonics generated by conductor positioning errors. Since LHC operates at a tune close to the third-integer resonance, the normal and skew sextupole errors in the inner triplet quadrupoles are

particularly dangerous. Based on simulation results and on measurement data from LBQ and HERA, the expected RMS spread $\sigma(b_3, a_3)$ is 1.3 units at the reference radius of 1 cm [5]. Figure 7 shows the a_3 and b_3 variation which can be obtained as function of the position of tuning shim 1 (first octant). For tuning shim 2 (second octant counter-clockwise), due to symmetry the curves for a_3 and b_3 are exchanged. With 8 tuning shims, corrections of both a_3 and b_3 in the range $\pm 3\sigma$ are possible. It should be noted, however, that due to saturation effects in order to achieve a given correction at nominal gradient an overcompensation of about a factor of two at injection is necessary. The tuning shim effect decreases rapidly for increasing multipole orders: the capability to correct normal and skew octupole drops to $\pm 1\sigma$ of the expected random variation, while no significant effect is observed for decapole and higher-order harmonics.

B. End Regions

In the magnet end regions, additional terms (pseudo-multipoles) are required in the harmonic expansion for the local field [19]. A simple expansion based on equation 1 can however be recovered for the integral of the transverse field, provided that the longitudinal field component vanishes at the boundaries of the integration interval. In this case, the pseudo-multipole components must integrate to zero and can therefore be eliminated. This condition is satisfied if the integral covers the whole end region, i.e. if the starting point z_p is sufficiently inside the magnet body and the end point z_q is sufficiently far away from the coil termination. As in the magnet straight section, the integrated multipole components in the end regions are expressed in units of 10^{-4} of the main integrated quadrupole field \hat{B}_2 . The magnetic length L_m of the interval $[z_p, z_q]$ is defined as the length of straight section which would provide an equivalent integrated gradient: $L_m = \hat{B}_2/B_2$.

TABLE IV

Integrated harmonic coefficients in the end regions of magnet models HGQS01 and HGQS02 at a reference radius of 1 cm.

Parameter	Return end		Lead end	
	HGQS02	HGQS01	HGQS02	HGQS01
L_m (cm)	32.50	31.78	41.39	40.72
\hat{b}_2	10000	10000	10000	10000
\hat{b}_6	0.140	0.048	0.657	0.597
\hat{b}_{10}	-0.0040	-0.0041	-0.0032	-0.0032
\hat{b}_{14}	-0.000017	-0.000017	-0.000015	-0.000015
\hat{a}_2			38.54	42.8
\hat{a}_6			0.020	0.025
\hat{a}_{10}			-0.0011	-0.0011
\hat{a}_{14}			0.000007	0.000006

Table IV shows the integrated multipole coefficients in the end regions of the two models. The integration limits are $[-25, +25]$ cm in the return end and $[-35, +25]$ cm in the lead end. The magnetic length calculation is relative to the low-current transfer function in the magnet body (18.22 T/m/kA). As can be expected, a slight increase in magnetic length is obtained with the modified end configuration. From the field quality standpoint, the

end configuration of HGQS02 is substantially equivalent to that of HGQS01: the \hat{b}_6 component is slightly higher in both the return and the lead end, while some reduction of the skew terms \hat{a}_2 and \hat{a}_6 in the lead end is observed. The change in the higher order terms ($n=10, 14$) of both the return and the lead end is negligible.

VI. CONCLUSIONS

The calculated maximum field gradient of the first two HGQ short models exceeds the LHC low- β quadrupole design specification of 200 T/m with a good margin. The short sample limit current for magnet model HGQS01 is 13.9 kA, corresponding to a gradient of 248 T/m. The short sample limit current for magnet model HGQS02 is 14.2 kA, corresponding to a gradient of 254 T/m. A modified end configuration in model HGQS02 allows to decrease the peak field in the outer layer with no significant degradation of the field quality.

REFERENCES

- [1] "Large Hadron Collider Conceptual Design", CERN/AC/95-05 (LHC), October 1995.
- [2] R. Ostojic, T. Taylor, S. Weisz, "Systems Layout of the Low- β Insertions for the LHC Experiments", 1997 Particle Accelerator Conference, Vancouver, Canada, May 1997.
- [3] R. Bossert et al., "Development of a High Gradient Quadrupole for the LHC Interaction Regions", 1996 Applied Superconductivity Conference, Pittsburgh, August 1996.
- [4] G. Sabbi, "Load lines and short sample limits for HGQ model S01", Fermilab TD-97-011, April 1997.
- [5] G. Sabbi, A. Zlobin, "Field Errors in the HGQ Straight Section", Fermilab TD-97-012, June 1997.
- [6] S. Caspi, K. Chow, "Normal and Skew Multipoles in the LHC Low Beta Quad - Rev. 1", LBL SC-MAG-577, February 1997.
- [7] G. Sabbi, "Magnetic Field Analysis of HGQ Coil Ends", Fermilab TD-97-040, September 1997.
- [8] G. Sabbi, "End Field Analysis of HGQ model S02", Fermilab TD-97-045, October 1997.
- [9] S. Caspi, "LHC IR Quad", Presented at the FNAL/LBL/CERN videoconference meeting, May 1st, 1996.
- [10] J. Brandt, A. Simmons, "Coil End Design for the LHC IR Quadrupole Magnet", Fermilab TS-96-013, November 1996.
- [11] S. Russenschuck, "A computer program for the design of superconducting accelerator magnets", Proc. ACES Symposium, Monterey, California, 1995 and CERN AT/95-39, September 1995.
- [12] S. Caspi, R. Schmidt, "PKLBL Programs User's Manual - Version 2.0", LBL-SC-MAG 471, August 1994.
- [13] R. Holsinger, C. Iselin, "The Cern-Poisson package user guide", Cern Program Library long writeup, August 1984.
- [14] S. Caspi, M. Helm, L. Laslett, V. Brady, "An approach to 3D Magnetic Field Calculation Using Numerical and Differential Algebra Methods", LBL SC-MAG-395, July 1992.
- [15] R. Scanlan et al, "Design and Fabrication of a High Aspect Ratio Cable for a High Gradient Quadrupole Magnet", ASC '96, Pittsburgh, August 1996.
- [16] A. Ghosh, private communication.
- [17] R. Hanft et al., "Magnetic Performance of New Fermilab High Gradient Quadrupoles", IEEE Particle Accelerator Conference (PAC91), S. Francisco, May 1991.
- [18] J. Perot, J. M. Rifflet, "Measurement Data Taken During the Industrial Fabrication of the HERA Superconducting Quadrupoles", Supercollider 3, Plenum Press, NY, 1991.
- [19] S. Caspi, M. Help, L. Laslett, "3D Field Harmonics", LBL Report SC-MAG-328, March 1991.